Prediction of water film depth on grooved airport runway induced by intense rainfall and wind

Kaihua Guo[1], Mengyao Wang[1], Xiao Feng[1], Haochen Yan[1], Yunfei Mao[1], Zhaofeng Han[1], Wai Lam Ng[1], Mingfu Guan[1*], Ji Chen[1*]

[1]Department of Civil Engineering, the University of Hong Kong, Hong Kong, 999077, HKSAR

[*] *Correspondence to*: Dr. Mingfu Guan (mfguan@hku.hk) and Prof. Ji Chen (jichen@hku.hk)

Abstract

The runway water film depth (WFD) and its drainage have direct impact on hydroplaning risk and, consequently, aircraft operational safety. Understanding its relationship with weather and runway conditions can help manage such risk due to WFD. Thus, this study develops an empirical formula to correlate runway risk area with its influencing factors using a dataset generated by a comprehensive rainfall-runoff dynamic model. The model incorporates a wind speed induced stress and is validated with physical experiment collected data. The simulation and observation showed good agreement, verifying the model's capability to reasonably well simulate the WFD distribution on intricate grooved surfaces at the millimetre level, with the consideration of wind effects. Then, this study performs 456 numerical experiments at the lateral prototype scale considering various rainfall intensity, wind speed, runway deterioration area, and groove depth. The impact of these factors on the peak WFD and the runway risk area is quantitatively analysed. The proposed empirical formula and developed dynamic model enables accurate assessment and prediction of the runway risk area under extreme weather conditions for better management of potential hydroplaning.

Keywords: Water film depth, Hydrodynamic model, Wind effect, Rainfall intensity, Runway deterioration

1. Introduction

While accidents on airport runways are relatively rare compared to other modes of transportation, their consequences can be severe and devastating, often resulting in numerous casualties. Hydroplaning or aquaplaning, which occurs when a runway becomes wet, especially during high-speed landings and take offs, is a significant contributing factor to these accidents (Qian and Wang, 2022; Toraldo et al., 2023; Van Es et al., 2001). Supporting data from the National Aerospace Laboratory (NLA) underscores that the risk of landing overrun accidents on wet runways is ten times higher than on dry runways (Van Es et al., 2001). Water film depth (WFD) is a fundamental parameter that contributes to the risk of hydroplaning (Kane et al., 2019; Zhu et al., 2021; He et al., 2023). Hydroplaning or aquaplaning occurs when water film exerting uplifting forces lead to complete tire detachment from the pavement (Tanner et al., 1981; Chen and Wang, 2022; Edmar Schulz et al., 2021). Using WFD as an indicator of runway slipperiness offers a more intuitive and convenient approach for airport management (Dreher and Horne, 1963; Luo et al., 2014). The International Civil Aviation Organization (ICAO) recommends a maximum allowable water film depth of 3 mm on airport runways (Icao,

2013). Intense rainfall resulting in the accumulation of substantial surface water on airport runways can disrupt aviation operations (Pasindu and Fwa, 2015). Therefore, accurately calculating and predicting the water film depth under various weather conditions are crucial aspects of evaluating runway safety and managing risks.

Efforts in predicting WFD on runway surfaces resulting from rainfall can be categorized into empirical models and hydrodynamic models. Empirical models are developed through regression analysis of experimental data to estimate WFD (Ross and Russam, 1968; Officials, 2011; Gallaway et al., 1979; Chesterton et al., 2006). Some studies also developed theoretical prediction models based on the geometric features of the surface. Luo and Li (2019) proposed a novel model for asphalt pavement that takes into account factors such as flow path length, slope, and texture depth to predict the dynamic process of WFD. Their model exhibits exceptional accuracy under local precipitation conditions compared to the Gallaway model and PAVDRN model. Similarly, Han et al. (2021) developed a model that considers road geometric characteristics to predict WFD under varying rainfall intensities. The simplicity, user-friendliness, and ability to swiftly estimate WFD have contributed to the widespread adoption of empirical equations. But they may lack a comprehensive understanding of the underlying physics and struggle to capture complex interactions or predict WFD accurately under new or extreme conditions. Besides, the development and refinement of these models also place a significant demand on observational data, which can be challenging to obtain through physical experiments.

Rainfall-runoff dynamic models offer advantages by providing results at every grid point in the solution domain, allowing for detailed simulations of fluid field characteristics. The two-dimensional Shallow Water Equations (2D SWEs) are commonly employed to model free surface flows. But there have also been efforts to apply SWEs to simulate runoff processes on runway or pavement surfaces. Some simplified models employ kinematic wave or simplified calculation methods to simulate the runway surface runoff (Escarameia et al., 2006; Wolff, 2013; Chen et al., 2017; Jeong and Charbeneau, 2010; Jiang et al., 2022; Alber et al., 2020b; Randall et al., 2008; Wang et al., 2022), but they may not fully capture the dynamic processes occurring on grooved surfaces when dynamic terms are neglected (Su et al., 2019; Guo et al., 2021). In contrast, models based on 2D full hydrodynamic equations have shown promise in providing accurate approximations but have seen limited application in simulating runway WFD distribution (Gómez et al., 2011; Xiao et al., 2021). Runway environments often feature very shallow water depths, at the order of millimetres, which pose high requirement on the model accuracy and stable numerical schemes (Randall et al., 2008; Ressel and Herrmann, 2008; Guan et al., 2013). The source terms for bottom slope and friction slope in SWEs must be treated robustly to guarantee convergence and numerical stabilities. Furthermore, it is crucial to consider the influence of wind to capture the realistic behaviour of water flow under strong wind conditions (Petraczek, 1975; Edmar Schulz et al., 2021), which is also overlooked in all these models. Thus it is valuable to develop a full hydrodynamic model that incorporates wind stress to accurately simulate the shallower surface water flow on airport runways in various weather conditions.

WFD on airport runways is influenced by various factors, including rainfall intensity, wind conditions, and runway condition (Yager, 1983; Xiao et al., 2021; Yu et al., 2020). Rainfall intensity determines the amount of water that falls onto the runway. During heavy rainstorms, the presence of strong winds can impact the distribution of water, causing it to concentrate in certain areas or disperse more evenly across the surface based on wind speed and direction (Horne, 1975). In addition to weather factors, the condition of the runway also plays a significant role in controlling water depths. The repeated traffic loading on runways leads to their deterioration over time, which are commonly observed as groove damage (Toraldo et al., 2023). These deformations can impact the distribution of water depth by affecting the drainage capabilities of the runway (Alber et al., 2020a; Javilla et al., 2017; Ling et al., 2021). Research with a wide range of scenarios and variables are challenging to replicate in physical experiments. Combining experiment tests with numerical modelling presents a promising approach to predict WFD (Alber et al., 2020b). Laboratory tests provide accurate and reliable data, serving as a basis for validating and calibrating numerical models. Numerical modelling complements experiments by simulating a wide range of scenarios and variables that are challenging to replicate physically. It enables to explore different conditions, accurately predict system behaviour under various environmental influence factors. However, the current understanding of the combined effects of these various factors on surface water depths on airport runways is limited. To enhance the understanding and effectively support timely warnings of adverse weather conditions at airports, it is necessary to conduct a detailed evaluation of the various influencing factors, finally enable to derive relationships between these variables and WFD.

Therefore, this study attempts to develop a hydrodynamic model to simulate the millimetre-scale thin-layer surface water flow on airport runways, considering the influence of wind stress force. The model is meticulously calibrated and validated using experimental data, ensuring its accuracy and reliability in representing the behaviour of water flow on runways. A total of 456 designed numerical experiments are performed on a prototype runway. These experiments serve to investigate the spatiotemporal dynamics of WFD and quantitatively analyse the influence of various contributing factors (rainfall intensity, wind speed, and groove deteriorations) on WFD. Besides, a relationship between WFD and these variables is derived based on the extensive simulation dataset.

2. Materials and method

This study used a combined method of physical experiments, numerical modelling and regression analysis. We first established a physical model, downscaled based on a prototype runway, observe WFD distribution among different rainfall intensity, wind and groove conditions. Secondly, we developed a two-dimensional Shallow Water Equations (2D SWEs) based hydrodynamic model, which was calibrated and validated with the experimental dataset. Then upscaled research of the prototype runway is carried out based on numerical experiments and the validated model for a comprehensive evaluation. A total of 456 simulation scenario are

designed and calculated. Finally, this study derived an empirical equation by combining all these simulation results. The methodology framework is illustrated in Figure 1.

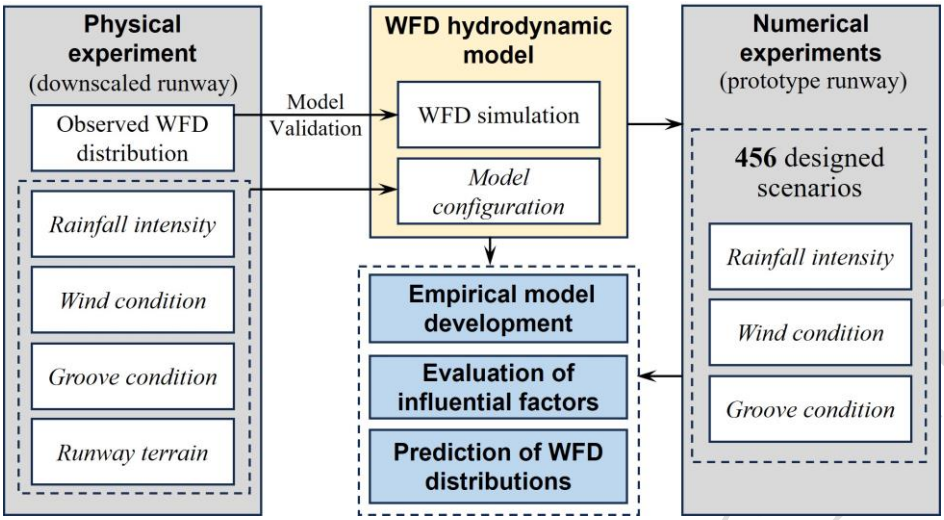

Figure 1. The framework of WFD prediction on grooved airport runway

2.1. Hydrodynamic model for WFD simulation

The 2D governing equations of the hydrodynamic model are expressed in vector form as below.

$$\frac{\partial \boldsymbol{Q}}{\partial t}+\frac{\partial \boldsymbol{F}}{\partial x}+\frac{\partial \boldsymbol{G}}{\partial y}=\boldsymbol{R}+\boldsymbol{S_b}+\boldsymbol{S_f}+\boldsymbol{S_w} \tag{1}$$

$$\boldsymbol{Q}=\begin{bmatrix} h \\ uh \\ vh \end{bmatrix} \quad \boldsymbol{F}=\begin{bmatrix} uh \\ u^2h+\frac{1}{2}gh^2 \\ uvh \end{bmatrix} \quad \boldsymbol{G}=\begin{bmatrix} vh \\ uvh \\ v^2h+\frac{1}{2}gh^2 \end{bmatrix} \tag{2}$$

$$\boldsymbol{R}=\begin{bmatrix} I \\ 0 \\ 0 \end{bmatrix} \boldsymbol{S_b}=\begin{bmatrix} 0 \\ -gh\frac{\partial b}{\partial x} \\ -gh\frac{\partial b}{\partial y} \end{bmatrix} \boldsymbol{S_f}=\begin{bmatrix} 0 \\ -C_f u\sqrt{u^2+v^2} \\ -C_f v\sqrt{u^2+v^2} \end{bmatrix} \boldsymbol{S_w}=\begin{bmatrix} 0 \\ \frac{c_{Dx}\rho_a}{\rho}u_w\sqrt{u_w^2+v_w^2} \\ \frac{c_{Dy}\rho_a}{\rho}v_w\sqrt{u_w^2+v_w^2} \end{bmatrix} \tag{3}$$

$$c_{Dx}=\begin{cases} 0.0012 & for\ u_w<7 \\ 0.0012\times\left(1+\frac{u_w-7}{18}\right) & for\ 7\le u_w\le 25 \\ 0.0024 & for\ u_w>25 \end{cases} \tag{4}$$

where x and y are the two Cartesian directions, t is time (s), $\boldsymbol{Q}$ is the vector representing the conserved flow variables, $\boldsymbol{F}$ and $\boldsymbol{G}$ are the flux vector terms in the x and y directions, respectively, $\boldsymbol{R}$ is the source or sink term representing net rainfall intensity, $\boldsymbol{S_b}$, $\boldsymbol{S_f}$ and $\boldsymbol{S_w}$ are the bed slope source term vectors, friction effect source term vectors and wind stress source term vectors, respectively, u and v are the x and y components of the flow velocity (m/s), b is the bed elevation (m), h is the water depth (m), g is the gravitational acceleration (m/s^2), I is rainfall intensity (m/s), C_f is the roughness coefficient, c_{Dx} and c_{Dy} stand for the wind stress coefficient in the x and y directions, respectively, ρ_a is the air density, u_w and v_w are the components of the wind velocity and it is 10-minute sustained wind speed acting 10 m above the surface (m/s), ρ denotes the density of water.

The model's governing equations (Eqs. (1), (2) and (3)) are solved numerically by a well-balanced Godunov-type finite volume method (FVM) on Cartesian grids. To achieve accurate and stable simulation for shallow water depths, this model applies the surface reconstruction method introduced by Xia et al. (2017) to discretize the bed slope source term $\boldsymbol{S_b}$. The friction source term, $\boldsymbol{S_f}$, is calculated using an implicit method proposed by Liang and Marche (2009) to achieve numerical stabilities when dealing with small water depths in combination with high friction slopes. The wind stress is determined using bulk parameterizations that estimate turbulent fluxes based on standard meteorological data. For the parameterization of the drag coefficient, the empirical formula proposed by Wu (1994) is employed. It considers the specific conditions of the wind field to enhance the accuracy of wind stress calculations, as shown in the Eq. (4) to calculate the drag coefficient in *x* direction. The calculation along the *y* direction is analogous, involving the variable v_w. Besides, the model utilizes an OpenMPI-accelerated approach to expedite the simulation, thereby maintaining a high model resolution while minimizing computational costs. The Harten, Lax and van Leer Riemann solver (HLL) is adopted to compute the fluxes of mass and momentum. The details can be found in previous publications (Guan et al., 2013; Guan et al., 2023; Guo et al., 2023).

The study primarily focused on immediate drainage processes and short-duration rainfall events when making predictions of WFD. Runway penetration exerts minimal influence and is disregarded. Accurately characterizing runway texture using terrain data at a 2mm scale remains a challenging task. The influence of runway texture on surface runoff processes is approximated using the Manning's coefficient. It remains acceptable as the model demonstrates good performance during validation. Despite the use of acceleration algorithms, computational efficiency may still fall short of real-time requirements for risk management and emergency response. To address this, we plan to develop an empirical model based on a substantial number of practical numerical experiments. This model will serve as a valuable tool to compensate for computational efficiency challenges.

2.2. Physical experiment configuration

A 6m by 4m physical model is built with concrete coated with a 50mm layer of Marshall asphalt. It is a downscaled based on the prototype of Hong Kong International Airport (HKIA) existing runway. The test report is provided as supplementary to certify the science and reliability. Within the upstream area spanning 4.8 meters, grooves measuring 6 mm by 6 mm with a spacing of 32 mm were implemented (Figure 2(a)), which is Federal Aviation Administration (FAA) standard groove configuration. This section had a slope of 1.5%. Conversely, within the downstream area spanning 1.2 meters, no grooves were present, and the slope was 2.5% (Figure 2(b)). To simulate rainfall events, a sprinkler system comprising six sprayers was installed around the model. The duration of each rainfall event was set at 5 minutes since this timeframe allowed for the stabilization of water film depth on the runway across all tested scenarios. Rainfall was generated through nozzle sprayers and the variation in rainfall intensity was achieved by adjusting the flow rates to each sprayer,

ranging from 600 to 1100 L/h, while keeping the intensity constant during the entire duration. 8 rain gauges were strategically positioned within the experimental area to measure distributed rainfall intensity.

In order to account for wind effects, the experiments considered the placement of blowers at the upstream and downstream ends of the runway slabs. This setup allowed for the generation of wind from different directions, corresponding to the upstream wind (upwind) and downstream wind (downwind). The wind speeds at various locations were measured using an anemometer positioned at a height of 8 cm. The observed wind speed range is 3.05-11.55 m/s. The relationship between the wind speeds at 8 cm and other heights could be determined by utilizing the wind profile under statically neutral conditions, as described by Stull (1988) in Eq. (5). Over time, the grooves on the runway surface deteriorate due to prolonged usage, leading to the inevitable formation of ruts. To represent runway rutting, rubber was filled into the grooves with a width of 350 mm at a distance of 3000 mm (Figure 2(c)). The same rainfall and wind conditions were replicated on both the surfaces with and without rubber filling, called 'Deterioration (DE)' scenario and 'No Deterioration (ND)' scenario, respectively. Water film thickness on the runway was measured along the central line in the 6-meter direction of the terrain.

$$\overline{U} = \frac{v_w}{\kappa} ln\left(\frac{z}{z_0}\right) \tag{5}$$

where κ=0.4 is Von Karman constant, $\overline{U}$ is the wind velocity profile, z_0 the observed height and v_w is the observed wind speed.

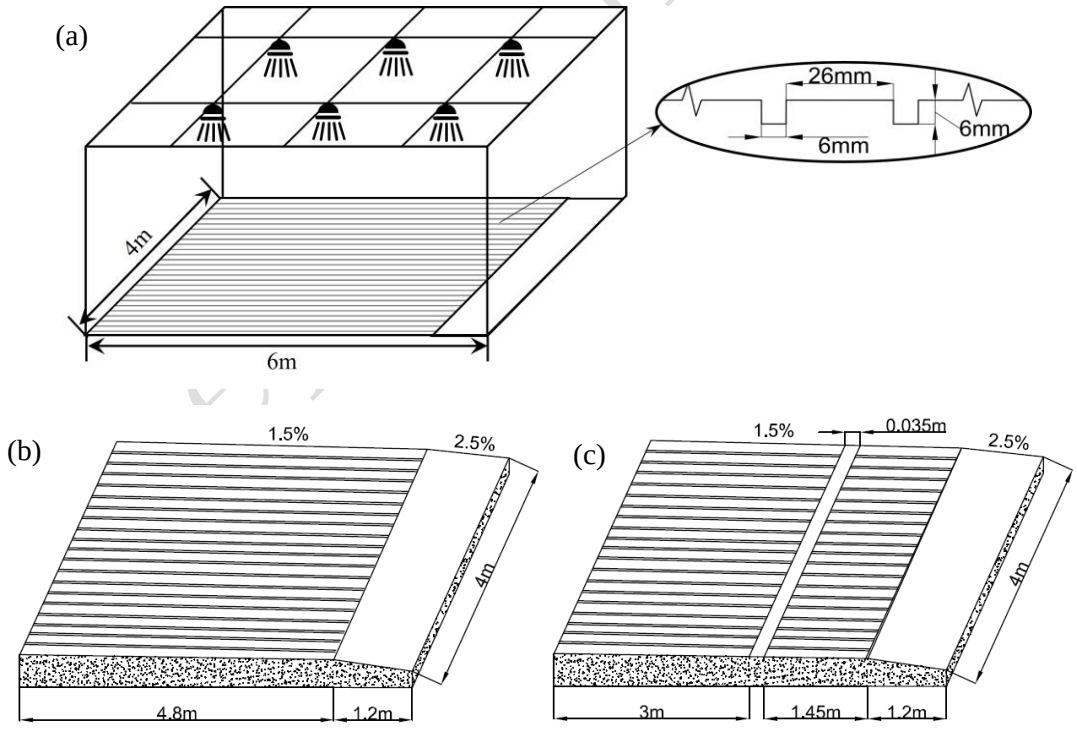

Figure 2. Schematic diagram of experimental design (a) and experiment surfaces: ND surface (b) and DE surface (c).

The manning's roughness plays a crucial role in hydraulic simulations. While the manning value for asphalt typically ranges from 0.010 to 0.016 according to the reference from Engineering Toolbox, it is important to

consider that this range is primarily applicable to rivers and other scenarios with larger water depth. Since the WFD in this study are very small, in the order of millimetres, adjustments to the manning's value are necessary. By utilizing the manning formula (Eq. (6) and (7)) and the continuity equation (Eq. (8)), the manning parameter can be calculated based on the WFD and the characteristics of the terrain, such as slope and width, in Eq. (9). Through analysis of the observed WFD ranges across various experimental scenarios, the range of the manning value in this study was determined as 0.012 to 0.020. Furthermore, as depicted in the Figure 3, there is a noticeable contrast in smoothness between the interior and exterior of the grooves, which necessitates the use of different manning coefficients to better characterize this feature. Specifically, a manning coefficient range of 0.012-0.018 is employed for the interior of the grooves, while the exterior region of the grooves utilizes a manning coefficient range of 0.013-0.020. This adjusted range considers the specific conditions of the study, ensuring more accurate and reliable hydraulic simulations.

$$v = C_f\sqrt{RJ} \tag{6}$$

$$C_f = \frac{1}{n}R^{1/6} \tag{7}$$

$$v = \frac{Q}{A} = \frac{Q}{bh} \tag{8}$$

$$n = \frac{bh}{Q}\left(\frac{bh}{b+2h}\right)^{2/3} J^{1/2} \tag{9}$$

where n is manning parameter, v is the average velocity of cross section, Q is the discharge of the cross section, C_f is the roughness coefficient, R is hydraulic radius, J is terrain slope, A is cross section area, b is the width of cross section.

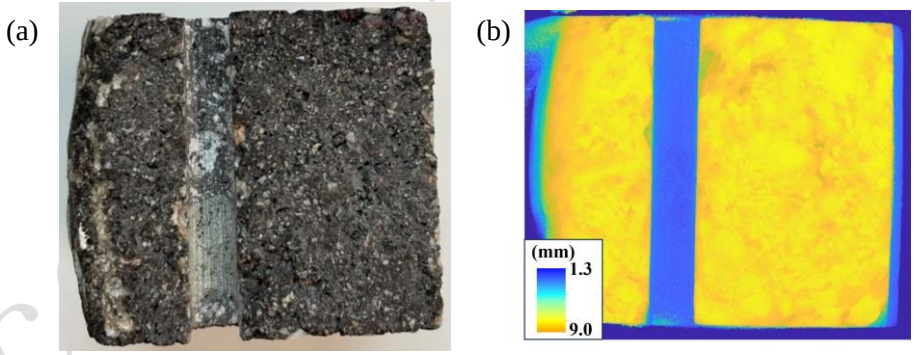

Figure 3. (a) The experimental runway sample (4cm×4cm) and (b) CT scanned surface elevation.

2.3. Numerical experiments design

Upscaled research of the prototype runway is carried out based on simulation experiments. The authentic and typical cross-sectional design of the airport runway exhibits symmetry, with a gradual decline in elevation from the centre to the sides. For the prototype-scale simulation, a crucial area directly involved in aircraft operations during take-off and landing is selected, specifically the 70-meter width section at the centre. The initial 30 meters on both sides of the centre exhibit a slope of 1.5%, followed by a slope of 2.5% from 30 meters to 37.5 meters. Beyond this range, the slope increases to 5% to represent the boundary slope. Standard

grooves are present within a 27-meter range on each side of the centre. Figure 4 illustrates the detailed information for the left portion of the simulation surface. To ensure adequate time for efficient water drainage, the simulation duration is set to 3 minutes during rainfall and 7 minutes without rainfall. 456 numerical experiments are designed (Table 1) for a comprehensive evaluation of the impact of rainfall intensity, wind speed, and groove deterioration on the distribution of WFD. Details and the foundational basis for the scenario design will be provided below.

The design of rainfall intensity is grounded in the Intensity-Duration-Frequency (IDF) relationship specific to Hong Kong. Rainfall intensity does not directly result whether an aircraft takes off. Extreme rainfall intensities with different return period from 2-year to 500-year, are comprehensively considered to encompass all conceivable conditions. For a 1-minute duration, the intensities range from 212 to 303 mm/h, while for a 5-minute duration, they range from 155 to 236 mm/h. Taking all these factors into account, a total of 7 rainfall scenarios are designed, with intensities ranging from 150 to 300 mm/h in increments of 25 mm/h. After testing, incremental increase in WFD for each rainfall event is approximately at 0.5 mm, which is suitable without imposing significant computational burdens.

Regarding wind conditions, this research primarily focuses on analysing the variation of WFD along the cross-section of the runway (width direction). The wind direction in the simulations is set to blow from one side edge of the runway to the opposite side edge, following the width direction. It is important to note that airport operations are suspended when the wind speed exceeds level 9 on the Beaufort scale. Consequently, 5 wind conditions are designed to represent the maximum wind speeds for Beaufort scale levels 0, 2, 4, 6, and 8, corresponding to wind speeds of 0 km/h, 12 km/h, 28 km/h, 50 km/h and 75 km/h, respectively. For airport runways, the scale is relatively small compared to the height and scale of the atmosphere and runway surface can be considered relatively flat. Therefore, the wind speed is assumed to be uniformly distributed across the study domain.

Different groove deterioration conditions are devised to assess its adverse impact on WFD. Referring to the guidelines (Administration(Faa), 2016), maintenance action is recommended when 40 percent of the grooves on the runway have a depth equal to or less than 3 mm, indicating a substantial reduction in their efficacy in preventing hydroplaning. This suggests that the groove depth can decrease by up to 50% of its original value, and the grooved area can be reduced by up to 40% of its initial area before necessitating maintenance intervention. Therefore, two factors, groove depth and deterioration area, are considered to characterize runway deterioration. Regarding the deterioration area, the most critical scenario occurs when the deterioration is concentrated in the central section of the runway. Consequently, 5 deterioration area (DA) is designed to encompass 0%, 10%, 20%, 30%, and 40% of the grooved area, extending from the centreline to both sides. 4 Groove depths (Gd) of 6 mm (representing standard groove depth), 5 mm, 4 mm, 3 mm were analysed representing varying amounts of groove depths that may occur after groove deterioration. Corresponding to the above, simulation events without groove deterioration are referred to as ‘ND’ scenarios while simulation events with groove deterioration are denoted as ‘DE’ scenarios.

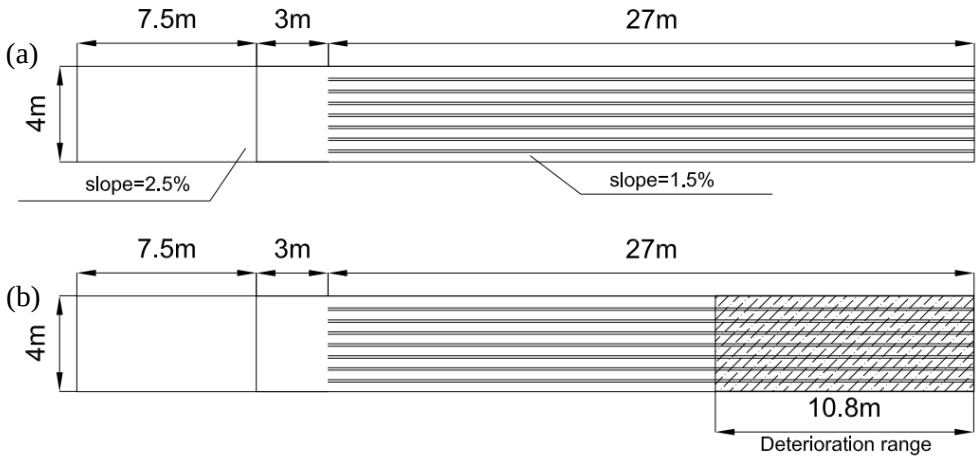

Figure 4. Left portion of ND scenario simulation area(a) and DE scenario simulation area(b).

Table 1. Designed simulation variables.

Designed variables	Values							Design basis
Rainfall intensity (mm/h)	150	175	200	225	250	275	300	IDF of Hong Kong
Wind speed (km/h)	0	12		28		50	75	Beaufort Wind Scale
Deterioration area (%)	0 (ND)	10 (DE)		20 (DE)		30 (DE)	40 (DE)	FAA standard
Groove depth (mm)	6 (ND)		5 (DE)		4 (DE)		3 (DE)	

3. Results and discussion

3.1 Validation of WFD hydrodynamic model

Three different rainfall events were selected for simulation, featuring flow rates of 700, 900, and 1100 L/h, under various conditions including wind and ruts. The corresponding average rainfall intensity are 141, 173 and 206mm/h, respectively. The grid precision in the computational domain is up to 2mm. The water film thickness at the peak time during the rainfall event with a flow rate of 700 L/h is illustrated in Figures 5 (additional figures can be found in the Appendix). It demonstrates the strong agreement between the simulated data and the observed data trend. The simulation results accurately capture the influence of the rutted area (DE scenario) and wind on WFD distribution. It provides strong validation for the model's capabilities in simulating runoff generation processes, handling complex flow stability, and incorporating the effects of wind. The comparison between the simulated WFD and the measured data is also evaluated using two performance metrics: the Nash-Sutcliffe Efficiency (NSE) coefficient and the Root Mean Squared Error (RMSE). The NSE and RMSE are defined by Eq. (10) and (11) respectively. From Figure 6, it can be observed that the NSE values for the different scenarios range from 0.58 to 0.94, all of which are greater than 0.5, indicating good agreement between the simulation results and the observed data. The RMSE values range from 0.30 to 0.70, indicating low prediction errors and high accuracy of the model. In Figure 6(c), The slope of prediction peak line was 0.99 which is very close to 1 (line of equality). The comparison further confirms the good agreement

between the simulation results and the observed data. This comprehensive evaluation demonstrates the model's competence in effectively handling the intricate topography of runways equipped with grooves and accounting for the influence of strong winds. The model successfully enables reliable simulation of the distribution of water film depth on real runways under diverse weather conditions and groove deterioration, thereby facilitating comprehensive risk assessment.

$$NSE = 1 - \frac{\sum_{i=1}^{n}\left(H_m^i - H_o^i\right)^2}{\sum_{i=1}^{n}\left(H_m^i - \overline{H_o}\right)^2} \tag{10}$$

$$RMSE = \sqrt{\frac{\sum_{i=1}^{n}\left(H_m^i - H_o^i\right)^2}{n}} \tag{11}$$

where $\overline{H_o}$ is the mean of observed water film depth; H_m^i is modeled water film depth, H_o^i is observed water film depth, n is the number of data.

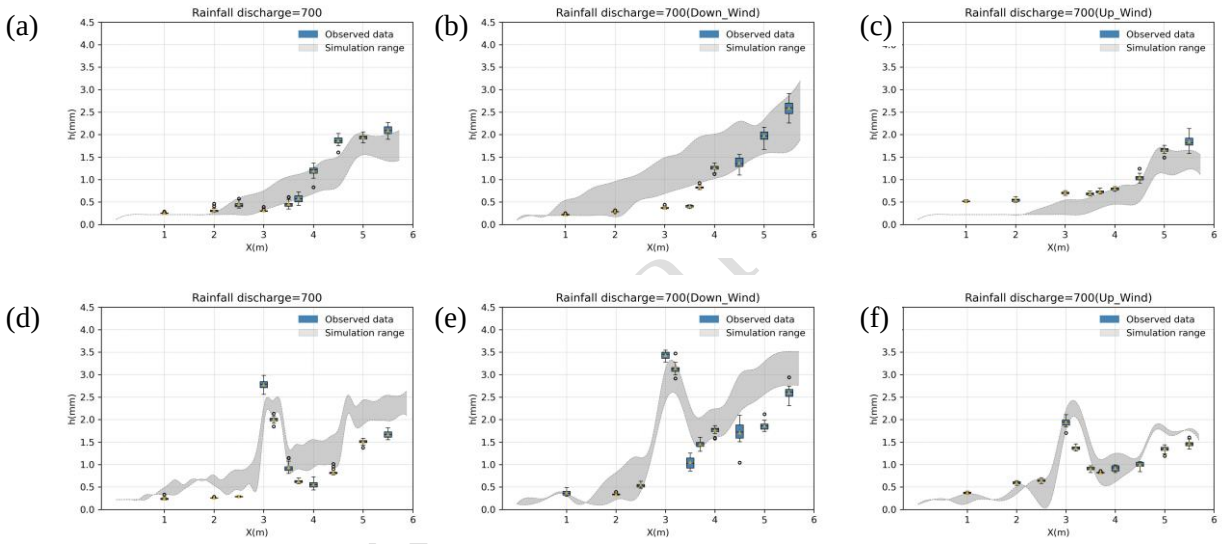

Figure 5. Simulated and measured WFD under the rainfall event with flow of 700L/h: (a) ND surface without wind, (b) ND surface with downwind, (c) ND surface with upwind, (d) DE surface without wind, (e) DE surface with downwind, (f) DE surface with upwind. Noted: the grey band denotes ensemble simulated results with a range of varying manning's roughness.

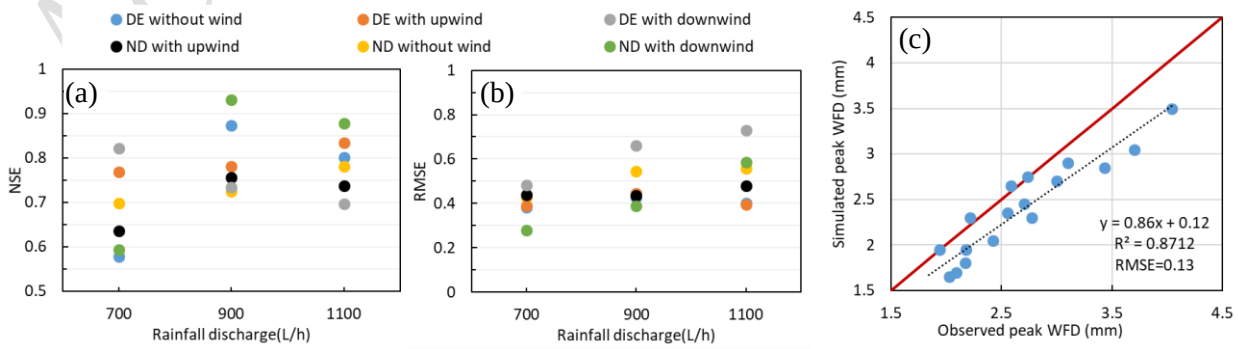

Figure 6. Calculated NSE values (a) and RMSE values (b) and the comparison between observed peak water film depth and simulated water film depth(c) of various scenarios.

3.2 Analysis of influential factors

3.2.1 Rainfall intensities effects on WFD distribution

Figures 7(a) and (b) depict the trend of WFD distribution on the runway under various Manning's roughness, using a rainfall intensity of 300 mm/h as a representative example. Along the longitudinal axis (in the 4m direction), where there is no slope, the water depth remains constant. Conversely, in the transverse axis (in the 70m direction), the water depth exhibits a symmetrical distribution that corresponds to the underlying topography. In Figure 7(c), the water depth distribution is depicted at the peak moment along the longitudinal cross-section. The water depth gradually increases as one moves downstream along the slope. Specifically, within a 30-meter span on both sides of the centreline, where the bottom slope measures 1.5%, a noticeable elevation in water depth can be observed at the point where the grooved and non-grooved areas converge. This observation can be attributed to the influence of the grooves, which effectively enhance the flow velocity of water. Conversely, in the downstream regions without grooves, the drainage process occurs at a relatively slower pace. Along the downstream area with a steeper bottom slope of 2.5%, beyond the aforementioned 30-meter range, there is a sudden and pronounced drop in water depth at the junction where these two bottom slopes meet, followed by a gradual increase. This can be attributed to the intensified incline, which fosters a more expeditious drainage process. It should be noted that the variation trend of the maximum and minimum values of the WFD is similar and the subsequent analysis will focus solely on the maximum value.

A significant and positive correlation is observed between the peak water depth and rainfall intensity, as demonstrated in Figure 8(a). The water depth exhibits remarkable sensitivity to variations in rainfall intensity, showing an approximate increase of 0.5mm for every increment in rainfall intensity. This relationship follows a consistent linear distribution, allowing it to be fitted into a linear equation with an r exceeding 0.99. Furthermore, RMSE is utilized to compare the temporal differences in the spatial distribution of WFD during simulations with various rainfall events, as depicted in Figure 8(b). The analysis reveals that the spatial and temporal variability of WFD distribution is concentrated primarily during the rainfall period (180s). As the rainfall diminishes and transitions into the drainage phase, the differences in WFD distribution gradually decrease. It is noteworthy that the discrepancies in WFD distribution diminish with an increase in rainfall intensity. In essence, the larger the rainfall intensity, the smaller the variation observed in the distribution of water depth. This suggests that even slight increments in rainfall intensity can result in considerable disparities in water depth distribution when dealing with lower rainfall intensities.

From a risk perspective, a critical WFD of 3mm is adopted (Administration(Faa), 2016), designating areas where the water depth exceeds this threshold as the "risk area." The proportion of the risk area relative to the groove area at the peak moment is quantitatively assessed, as depicted in Figure 8(a). With an escalation in rainfall intensity, the proportion of the risk area gradually expands, albeit at a diminishing rate. This implies that as the rainfall intensity increases, the impact of a similar increment in water depth on the risk area gradually diminishes. In other words, at lower rainfall intensities, an increase in water depth may result in a substantial expansion of the risk area. However, as rainfall intensities reach higher levels, the extension of the risk area

due to equivalent increments in water depth may become less prominent. In summary, the sensitivity of the risk area proportion to rainfall intensity diminishes as the intensity itself increases.

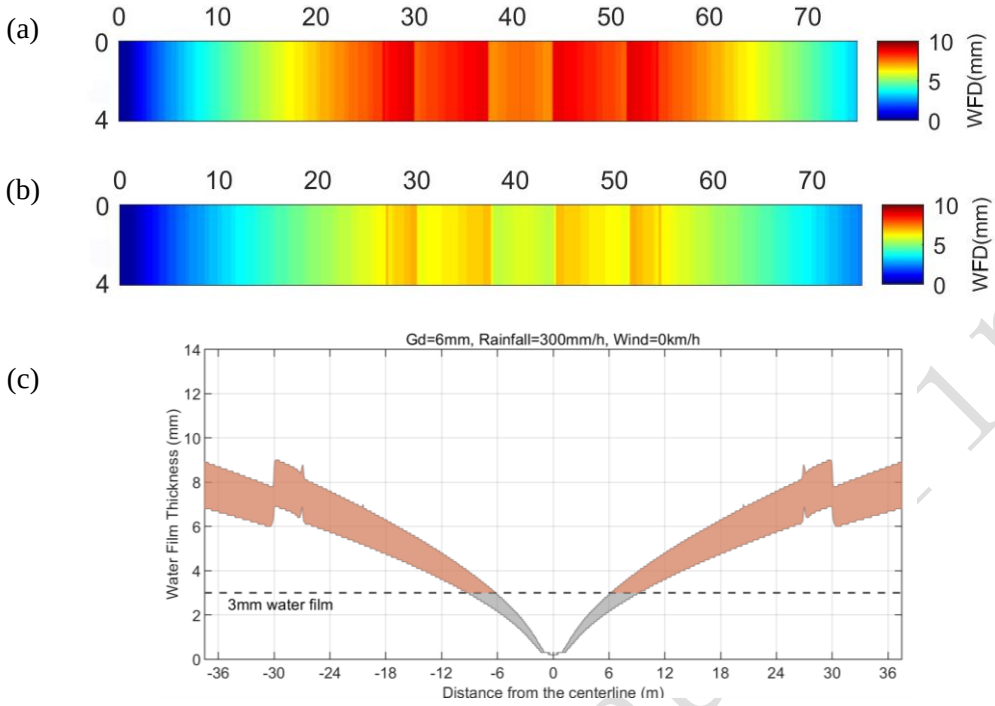

Figure 7. (a) The plan view of WFD distribution at peak time with the upper limit of the Manning's coefficient and (b) the lower limit of the Manning's coefficient; (c) the cross-sectional view of WFD distribution on the runway surface.

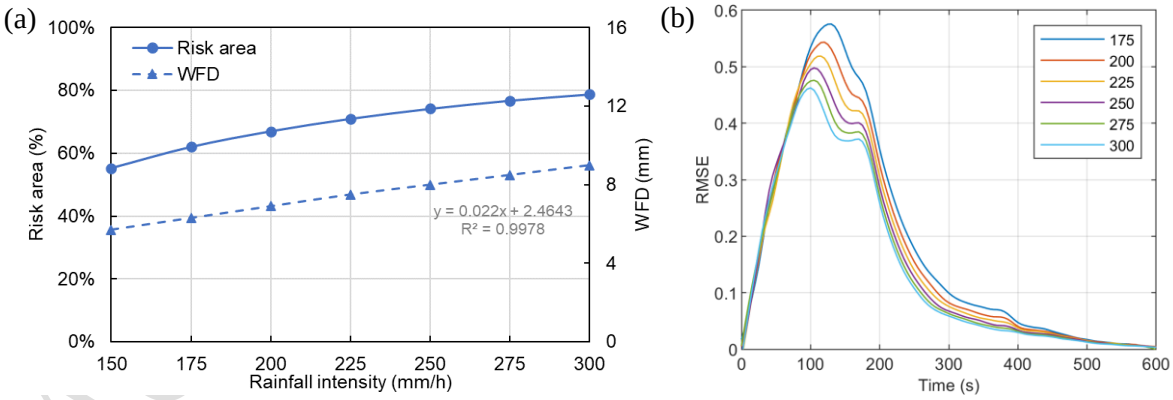

Figure 8. (a) The peak WFD and the proportion of risk area with varying rainfall intensities, and (b) the temporal variation of RMSE for the WFD simulated with the six rainfall intensities.

3.2.2 Wind effects on WFD distribution

Due to the symmetrical nature of the runway terrain, it enables the observations of WFD distribution under headwind and tailwind conditions in the left and right halves of the runway, respectively. Figure 9 depicts the water depth distribution at a rainfall intensity of 300 mm/h, revealing an asymmetric phenomenon. In the right half of the runway, where the wind direction aligns with the slope, the water flow is accelerated by the wind,

resulting in lower WFD values. Conversely, in the left half of the runway, where the wind direction opposes the slope, the water flow is impeded by the wind, leading to higher WFD values. Consequently, in comparison to the windless scenario, the presence of wind amplifies the peak values of WFD, consistently localized on the left side of the runway. But the wind force does not affect the location of the WFD peak.

As shown by the dashed line in Figure 10(a), there is a slight increase in the rate of WFD peak growth as the wind speed rises. However, this increase is minimal, with the difference in growth rate between the highest and lowest wind speed scenarios being less than 1 mm for all precipitation events. The WFD peak showcases a restrained responsiveness to alterations in wind speed. The trend of WFD growth remains consistent across different rainfall intensities, indicating a similar impact of wind speed on WFD regardless of precipitation intensity. For the risk area, the presence of wind speeds below 50 km/h shows slight increase compared to the no-wind scenario, which remains smaller than 1% for all rainfall events. However, as the wind speed reaches 75 km/h, a significant rise in the risk area is observed, ranging from 6% to 11%. Even minimal fluctuations in WFD can lead to a significant expansion in the risk area in high wind speed conditions. And the extent of this increase diminishes as the rainfall intensity becomes higher. Figure 10(b) displays the RMSE values, which measure temporal differences in the spatial distribution of WFD under varying wind speeds. Similarly, the influence of wind speed on WFD distribution becomes significantly more pronounced at higher wind speeds (75km/h). It is noteworthy that within the duration of rainfall (180s), the RMSE stays below 0.5. Following the conclusion of rainfall, there is a distinct surge in RMSE, especially in the scenario involving a wind speed of 75 km/h. This signifies that the influence of wind speed on WFD is predominantly concentrated during the subsequent drainage phase after precipitation. In summary, the WFD peak exhibits limited sensitivity to wind speed fluctuations. However, when confronted with strong winds of level 8 or higher, the WFD distribution undergoes a significant influence, including a deceleration in the drainage process and a notable increase in the risk area.

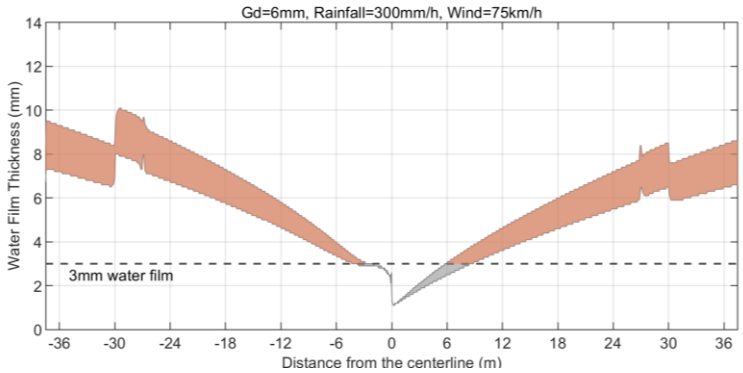

Figure 9. The cross-sectional view of WFD distribution with wind

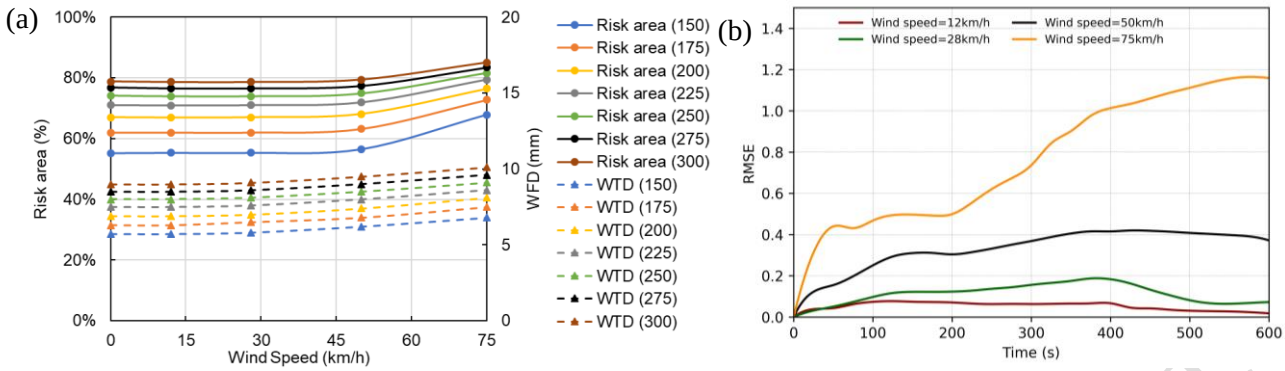

Figure 10. (a) The extracted peak WFD and the proportion of risk area with varying wind speed and (b) the temporal difference between the spatial distribution of WFD with rainfall intensity of 300mm/h.

3.2.3 Grooves deterioration effects on WFD distribution

Deterioration is characterized by two parameters: the deterioration area (DA) and groove depth (Gd). Figure 11 illustrates the distribution of water depth at a rainfall intensity of 300 mm/h for a DA of 10% and Gd of 3mm. The deterioration adversely affects the runway's drainage capacity and led to an increase in overall water depths, particularly within the deteriorated area. However, it's important to note that the position of the WFD peak remained constant. For WFD peak, the observed increase is relatively minor (≤0.2mm) and variations in wind speed and rainfall intensity do not exacerbate this phenomenon, as depicted in Figure 12(a) and (c). Figure 12(d) presents the RMSE of the WFD distribution over time under different deterioration conditions. With various DA values, the spatial variations in the distribution are most pronounced with relatively smaller WFD, during the initial precipitation phase and the latter stage of the drainage phase. However, varying Gd exhibit a positive correlation emerges between the RMSE and water depth. As the water depth increases, the RMSE also increases. Conversely, during the latter portion of the drainage phase, as the water depth decreases, the RMSE gradually decreases as well.

Regarding the risk area, Figures 12(b) and (c) illustrate the fluctuations under various deterioration conditions, taking into account additional factors. An increase in Gd resulted in a consistent linear reduction in the risk area. This effect became more pronounced when combined with an expanded DA, resulting in a range of 2% to 10%. This pattern held steady across diverse rainfall intensities and wind speeds. In the case of DA, the transition from 10% to 20% exerted a more substantial impact on the risk area compared to further increments. This suggests that the most significant influence on the risk area occurs during the initial transition from a smaller DA to a slightly larger one, and subsequent deterioration beyond that point (approximately 20%) does not significantly contribute to the expansion of the risk area. Increased rainfall intensity tends to mitigate the influence of deterioration on the risk area. In essence, as the rainfall intensity increases, the risk area becomes substantial. The additional impact of the deterioration area on the risk area becomes less significant, resulting in a smaller percentage increase in the risk area. And the impact of DA outweighs that of Gd with smaller rainfall intensity. However, when confronted with strong winds (75 km/h), the influence of deterioration on the risk area is significantly magnified. And the impact of Gd takes precedence over that of DA.

In summary, the peak value of WFD remains insensitive to deterioration. However, deterioration can significantly impact the risk area, especially in scenarios with strong winds. Combining 150mm/h rainfall intensity with strong wind speed and acceptable deterioration, risk area can be expanded to 80%. Therefore, even the groove condition being within the range that typically does not necessitate maintenance action, enhanced oversight of runway risks is imperative. It is advisable to uphold the optimal groove condition within operational limits.

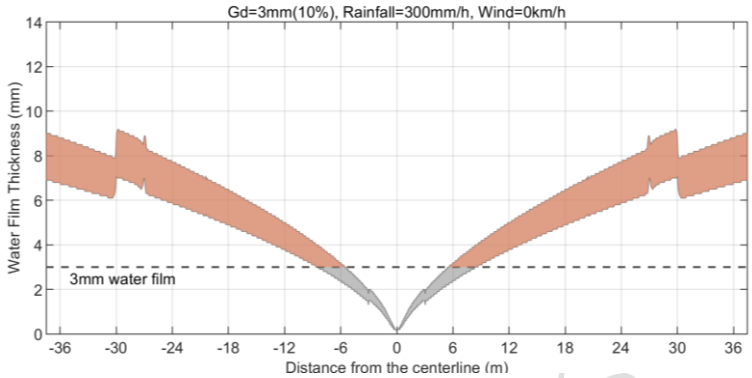

Figure 11. The cross-sectional view of WFD distribution with groove deterioration

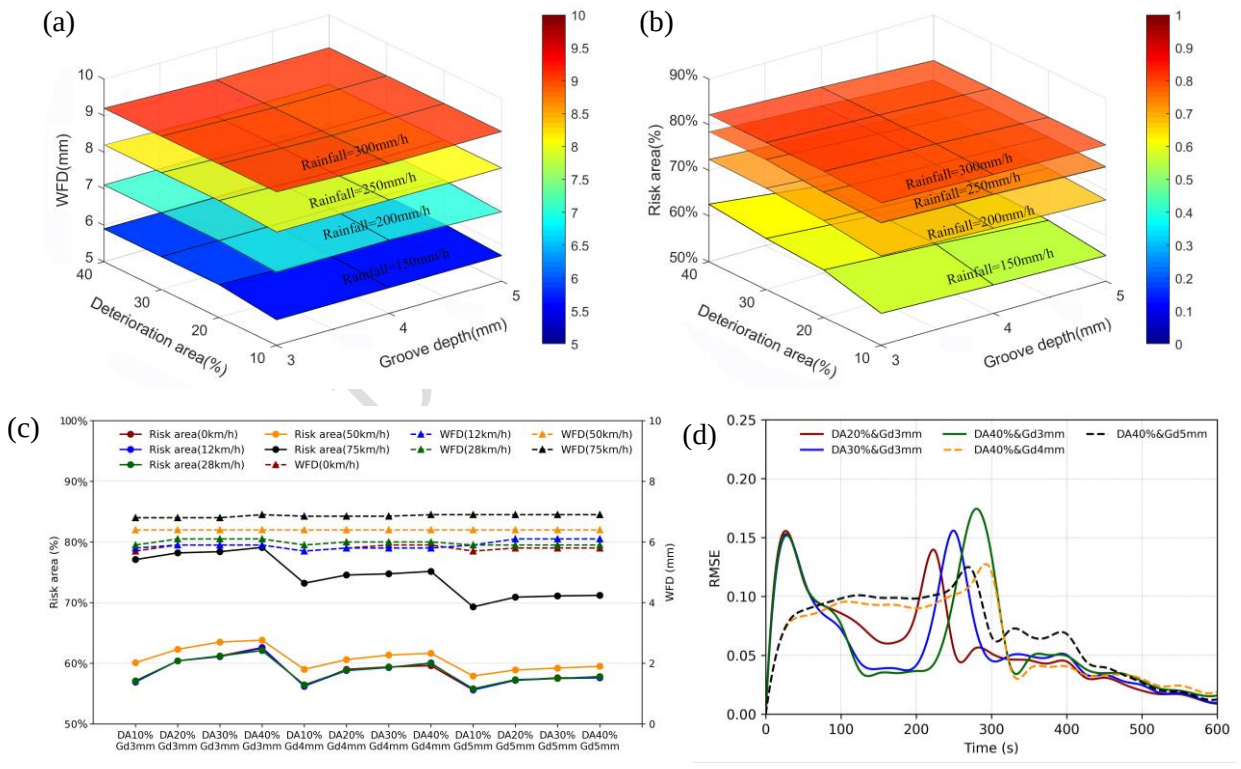

Figure 12. The extracted peak WFD (a) and the proportion of risk area (b) of different rainfall intensity and (c) the extracted peak WFD and the proportion of risk area of different wind speed with varying deterioration conditions and (d) The temporal difference between the spatial distribution of WFD with rainfall intensity of 150mm/h.

3.3 Correlation of runway risk area and influential factors

The simulation scenario aims to encompass a comprehensive range of adverse weather conditions and runway deterioration situations that an aircraft may encounter during operation. In contrast to the peak of WFD, the risk area provides a more intuitive depiction of the overall runway condition and its impact on aircraft take-off and landing. This section will further compare the effects of various influencing factors on the risk area and analyse which factor the risk area is more sensitive to, meaning that an increase in that specific factor poses a greater danger to aircraft operations. The analysis process involved normalizing the factors and conducting regression analysis. In the normalization section, the Min-Max Scaling method was employed. The regression model aimed to estimate the coefficients associated with each factor, indicating the direction and magnitude of their impact on the risk area. In the regression analysis, which yielded an R-squared value of 0.85, the coefficients for rainfall intensity, wind speed, deterioration area, and groove depth were 0.20, 0.09, 0.02, and -0.03, respectively. Notably, the impact of rainfall intensity appears to be the most significant, followed by wind speed, while the influences of deterioration area and groove depth are relatively smaller. It is consistent to the preceding analysis. These findings provide valuable insights for prioritizing mitigation strategies, with a particular emphasis on managing high rainfall intensities and wind speeds to minimize the risk area of the runway.

Based on all 456 simulation scenarios, a function was fitted based on multivariate nonlinear regression analysis to describe the relationship between the risk area and the variables of rainfall intensity, wind speed, deterioration area, and groove depth. This regression function achieved an impressive R-squared value of 0.96, indicating a strong fit to the data. Figure 13 presents the comparison between the predicted risk area derived from the regression equations and the simulated risk area across the 456 scenarios. By relying on established patterns and observed data, the empirical formula offers a more perceptible and straightforward method, enables efficient and rapid assessments of risk area under various factors. Its practicality and ease of use enhance its applicability in time-sensitive situations, allowing for timely decision-making and proactive measures to ensure the safety and efficiency of airport operations.

$$Ra = 0.8842i^{0.15} + (0.0062w^3 - 0.3309w^2 + 3.6392w) \times 10^{-4} \\ -0.0125Gd + 0.0005DA - 1.2290 \quad (12)$$

Where Ra is risk area percentage, i is rainfall intensity, mm/h, w is wind speed, km/h, Gd is groove depth, mm, DA is deterioration area percentage.

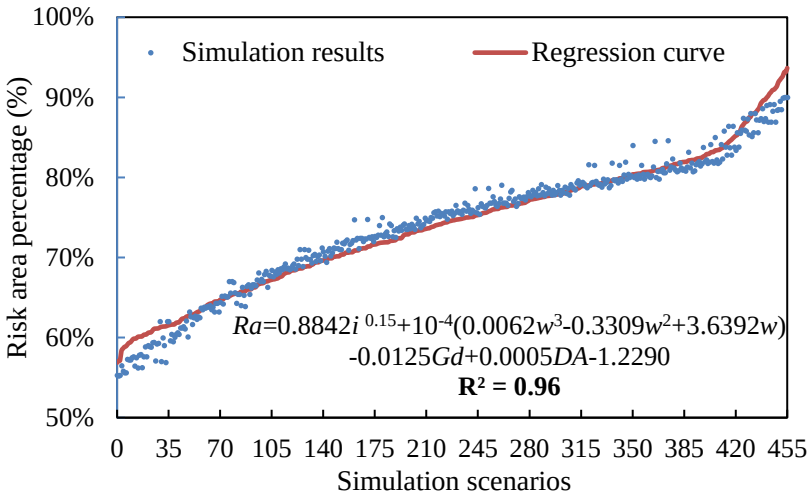

Figure 13. The comparison between the predicted risk area from the regression equations and the simulated risk area across the 456 scenarios.

4. Conclusion

This study develops a rainfall-runoff hydrodynamic model that integrates wind effects to simulate the rainfall-induced WFD on grooved runways. The model is well calibrated and validated using experimental data obtained from a downscaled physical model that faithfully replicates the geometric characteristics of an existing runway prototype. It enables the model to successfully capture the distribution of WFD associated with different levels of rainfall intensity, wind conditions, and groove deterioration. The evaluation metrics, including the NSE and RMSE, further affirm the model's reliability and accuracy. We then present an empirical model to predict the runway risk area under the effects of rainfall intensity, wind speed, deterioration area, and groove depth regressed based on a dataset generated from 456 simulations on a scaled-up lateral prototype. The development of the hydrodynamic model and empirical model facilitates accurate and prompt decision-making and runway risk management.

In addition, these numerical experiments allowed for a comprehensive quantitative analysis of the spatiotemporal distribution of WFD, providing valuable insights for runway risk management and maintenance recommendations. Among the factors considered, rainfall intensity stands out as a primary concern in runway risk management due to its significant influence on the runway's risk area. However, its sensitivity to risk area and peak WFD decreases as rainfall intensity increases. Interestingly, variations in wind speed and groove deterioration have a relatively minor impact on WFD peak. Nonetheless, when subjected to strong winds, the drainage process decelerates, accentuating the influence of these factors and leading to a substantial expansion of the risk area. It is essential to enhance runway risk monitoring during strong wind conditions, even in the presence of light rainfall and acceptable groove deterioration. Besides, upholding the optimal groove condition to the greatest extent possible is recommended.

Authorship contribution statement

KG: Conceptualization, Methodology, Investigation, Formal analysis, Data curation, Writing – original draft; MW: Methodology, Investigation, Writing – review & editing; XF: Methodology, Investigation; HY: Investigation, Data curation; YM: Investigation; ZH: Investigation; WN: Investigation; MG: Conceptualization, Methodology, Funding acquisition, Supervision, Writing – review & editing; JC: Conceptualization, Methodology, Funding acquisition, Supervision, Writing – review & editing.

Declaration of competing interest

The authors declare that they have no conflict of interest.

Acknowledgement

The study is financially supported by Early Career Scheme from Hong Kong University Grant Committee (grant number: 27202419), and SZ-HK-Macau Technology Research Programme (Type C) (grant number: SGDX20210823103537035).

References

Administration(FAA), F. A.: Measurement and Maintenance of Skid-Resistant Airport Pavement Surfaces, Federal Aviation Administration(FAA), Washington, 2016.

Alber, S., Schuck, B., and Ressel, W.: Importance of pavement drainage and different approaches of modelling, in: Functional Pavements, CRC Press, 403-406, 2020a.

Alber, S., Schuck, B., Ressel, W., Behnke, R., Falla, G. C., Kaliske, M., Leischner, S., and Wellner, F.: Modeling of Surface Drainage during the Service Life of Asphalt Pavements Showing Long-Term Rutting: A Modular Hydromechanical Approach, Advances in Materials Science and Engineering, 2020, http://dx.doi.org/10.1155/2020/8793652, 2020b.

Chen, X. and Wang, H.: Analysis and mitigation of hydroplaning risk considering spatial-temporal water condition on the pavement surface, International Journal of Pavement Engineering, http://dx.doi.org/10.1080/10298436.2022.2036988, 2022.

Chen, X., Geng, Y., Jiang, Q., Huang, X., and Ma, Y.: Innovative approach for pavement runoff characterization, Journal of Performance of Constructed Facilities, 31, 04017047, 2017.

Chesterton, J., Nancekivell, N., and Tunnicliffe, N.: The use of Gallaway equation for aquaplaning evaluation in New Zealand, Proc. NZIHT and Transit NZ 8th Annual Conference,

Dreher, R. C. and Horne, W. B.: Phenomena of pneumatic tire hydroplaning, The National Aeronautics and Space Administration (NASA), 1963.

Edmar Schulz, H., Edgar Curry, J., and Andrade Simões, A. L.: Water Films and Hydroplaning on Highways: Hydrodynamic Aspects, Journal of Transportation Engineering, Part B: Pavements, 147, 04021053, 2021.

Escarameia, M., Gasowski, Y., May, R., and Bergamini, L.: Estimation of runoff depths on paved areas, Urban Water Journal, 3, 185-197, 2006.

Gallaway, B. M., Hayes, G., Ivey, D., Ledbetter, W., Olson, R., Ross Jr, H., Schiller Jr, R., and Woods, D.: Pavement and geometric design criteria for minimizing hydroplaning. A technical summary, Final Report Texas A&M Univ, 1979.

Gómez, M., Macchione, F., and Russo, B.: Methodologies to study the surface hydraulic behaviour of urban catchments during storm events, Water Science and Technology, 63, 2666-2673, https://doi.org/10.2166/wst.2011.174, 2011.

Guan, M., Wright, N., and Sleigh, P.: A robust 2D shallow water model for solving flow over complex topography using homogenous flux method, International Journal for Numerical Methods in Fluids, 73, 225-249, https://doi.org/10.1002/fld.3795, 2013.

Guan, M., Guo, K., Yan, H., and Wright, N.: Bottom-up multilevel flood hazard mapping by integrated inundation modelling in data scarce cities, Journal of Hydrology, 129114, https://doi.org/10.1016/j.jhydrol.2023.129114, 2023.

Guo, K., Guan, M., Yan, H., and Xia, X.: A spatially distributed hydrodynamic model framework for urban flood hydrological and hydraulic processes involving drainage flow quantification, Journal of Hydrology, 130135, 2023.

Guo, K. H., Guan, M. F., and Yu, D. P.: Urban surface water flood modelling - a comprehensive review of current models and future challenges, Hydrology and Earth System Sciences, 25, 2843-2860, https://doi.org/10.5194/hess-25-2843-2021, 2021.

Han, S., Xu, J. L., Yan, M. H., Gao, S. J., Li, X. F., Huang, X. J., and Liu, Z. X.: Predicting the water film depth: A model based on the geometric features of road and capacity of drainage facilities, Plos one, 16, http://dx.doi.org/10.1371/journal.pone.0252767, 2021.

He, Y., Yang, X., Xiao, S., Liu, P., Lu, G., Xing, C., Fan, Z., Sheng, W., and Wang, D.: Experimental study on the high-speed frictional behavior between the tire and asphalt pavement, Construction and Building Materials, 371, 130782, 2023.

Horne, W. B.: Wet runways, 1975.

ICAO: the Convention of International Civil Aviatio, International Civil Aviation Organization, Montreal, 2013.

Javilla, B., Mo, L., Hao, F., Shu, B., and Wu, S.: Significance of initial rutting in prediction of rutting development and characterization of asphalt mixtures, Construction and Building Materials, 153, 157-164, 2017.

Jeong, J. and Charbeneau, R. J.: Diffusion wave model for simulating storm-water runoff on highway pavement surfaces at superelevation transition, Journal of Hydraulic Engineering, 136, 770-778, 2010.

Jiang, B. Y., Chen, X., and Wang, H.: Computational analysis of skid resistance of aircraft tire on wet runway pavement with different groove depths, Road Materials and Pavement Design, http://dx.doi.org/10.1080/14680629.2022.2092025, 2022.

Kane, M., Do, M.-T., Cerezo, V., Rado, Z., and Khelifi, C.: Contribution to pavement friction modelling: An introduction of the wetting effect, International Journal of Pavement Engineering, 20, 965-976, 2019.

Liang, Q. and Marche, F.: Numerical resolution of well-balanced shallow water equations with complex source terms, Advances in Water Resources, 32, 873-884, https://doi.org/10.1016/j.advwatres.2009.02.010, 2009.

Ling, J., Ren, L., Tian, Y., Gao, J., and Man, L.: Analysis of airfield composite pavement rutting using full-scale accelerated pavement testing and finite element method, Construction and Building Materials, 303, 124528, 2021.

Luo, W., Wang, K. C., Li, L., Li, Q. J., and Moravec, M.: Surface drainage evaluation for rigid pavements using an inertial measurement unit and 1-mm three-dimensional texture data, Transportation Research Record, 2457, 121-128, 2014.

Luo, W. T. and Li, L.: Development of a new analytical water film depth (WFD) prediction model for asphalt pavement drainage evaluation, Construction and Building Materials, 218, 530-542, http://dx.doi.org/10.1016/j.conbuildmat.2019.05.142, 2019.

Officials, T.: A Policy on Geometric Design of Highways and Streets, AASHTO2011.

Pasindu, H. and Fwa, T.: Improving wet-weather runway performance using trapezoidal grooving design, Transportation in developing economies, 1, 1-10, http://dx.doi.org/10.1007/s40890-015-0001-6, 2015.

Petraczek, O.: Experimentelle Ermittlung der Wasserfilmdicken auf Fahrbahnen unter natürlichen Bedingungen, FORSCH STRASSENBAU U STRASSENVERKEHRSTECH, 1975.

Qian, J. Y. and Wang, H.: Analysis of skid resistance and braking distance of aircraft tire landing on grooved runway pavement, International Journal of Pavement Engineering, http://dx.doi.org/10.1080/10298436.2022.2101054, 2022.

Randall, J. C., Jaehak, J., and Michael, E. B.: Highway Drainage at Superelevation Transitions, Center for Transportation Research at The University of Texas, Austin, 2008.

Ressel, W. and Herrmann, S.: Aquaplaning und Verkehrssicherheit in Verwindungsbereichen dreistelliger Richtungsfahrbahnen-Berechnung der Wasserfilmdicke, Forschung Straßenbau und Straßenverkehrstechnik, 2008.

Ross, N. and Russam, K.: The depth of rain water on road surfaces, 1968.

Stull, R. B.: An introduction to boundary layer meteorology, Springer Science & Business Media1988.

Su, B., Huang, H., and Zhu, W.: An urban pluvial flood simulation model based on diffusive wave approximation of shallow water equations, Nordic hydrology, 50, 138-154, https://doi.org/10.2166/nh.2017.233, 2019.

Tanner, J. A., Stubbs, S. M., and Smith, E. G.: Behavior of aircraft antiskid braking systems on dry and wet runway surfaces: Hydromechanically controlled system, 1981.

Toraldo, E., Ketabdari, M., Battista, G., and Crispino, M.: Assessing the Impact of Rutting Depth of Bituminous Airport Runway Pavements on Aircraft Landing Braking Distance during Intense Precipitation, Designs, 7, 41, 2023.

Van Es, G., Roelen, A., Kruijsen, E., and Giesberts, M.: Safety aspects of aircraft performance on wet and contaminated runways, 2001.

Wang, K., Li, P., Ai, Q., and Wei, X.: Study on water distribution characteristics of surface gathered water and water film thickness model, Alexandria Engineering Journal, 61, 3293-3302, 2022.

Wolff, A.: Simulation of Pavement Surface Runoff using the Depth-Averaged Shallow Water Equations, Institut für Straßen- und Verkehrswesen, Universitat Stuttgart, Stuttgart, 174 pp., 2013.

Wu, J.: The sea surface is aerodynamically rough even under light winds, Boundary-layer meteorology, 69, 149-158, 1994.

Xiao, W., Hui, C., Dong, N., and Jing, Z.: Study on hydrodynamic characteristics and influence factors of asphalt pavement runoff, Water Science and Technology, 84, 3928-3940, 2021.

Yager, T.: Review of factors affecting aircraft wet runway performance, 21st Aerospace Sciences Meeting, 274,

Yu, M., You, Z., Wu, G., Kong, L., Liu, C., and Gao, J.: Measurement and modeling of skid resistance of asphalt pavement: A review, Construction and Building Materials, 260, 119878, 2020.

Zhu, X. Y., Yang, Y., Zhao, H. D., Jelagin, D., Chen, F., Gilabert, F. A., and Guarin, A.: Effects of surface texture deterioration and wet surface conditions on asphalt runway skid resistance, Tribology International, 153, http://dx.doi.org/10.1016/j.triboint.2020.106589, 2021.

Appendix

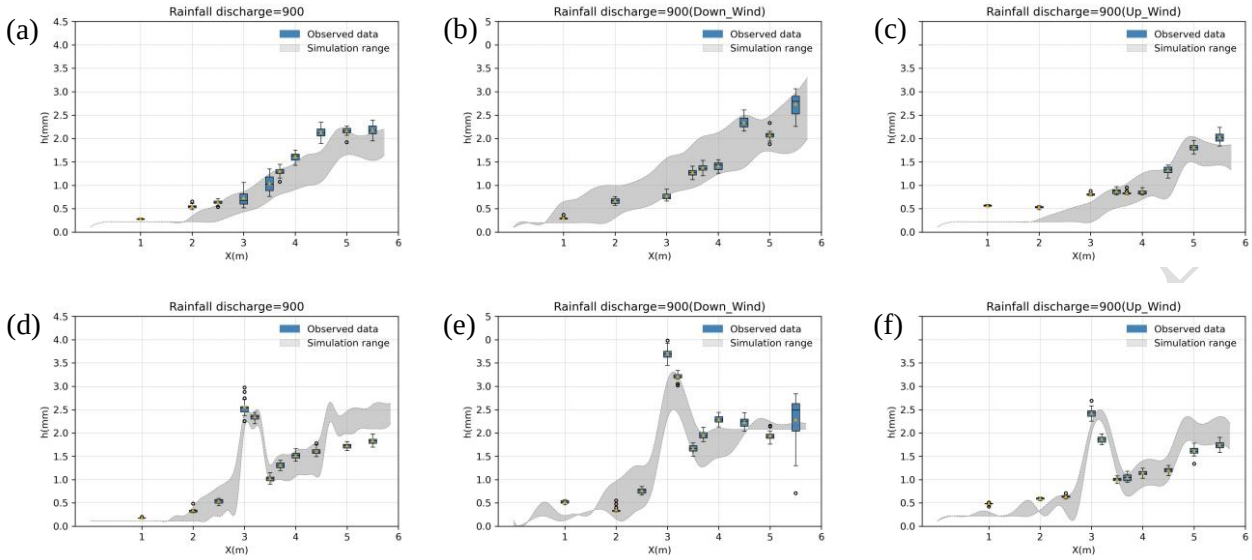

Figure A1. Simulated and measured WFD under the rainfall event with flow of 900L/h: (a) ND surface without wind, (b) ND surface with downwind, (c) ND surface with upwind, (d) DE surface without wind, (e) DE surface with downwind, (f) DE surface with upwind. Noted: the grey band denotes ensemble simulated results with a range of varying manning's roughness.

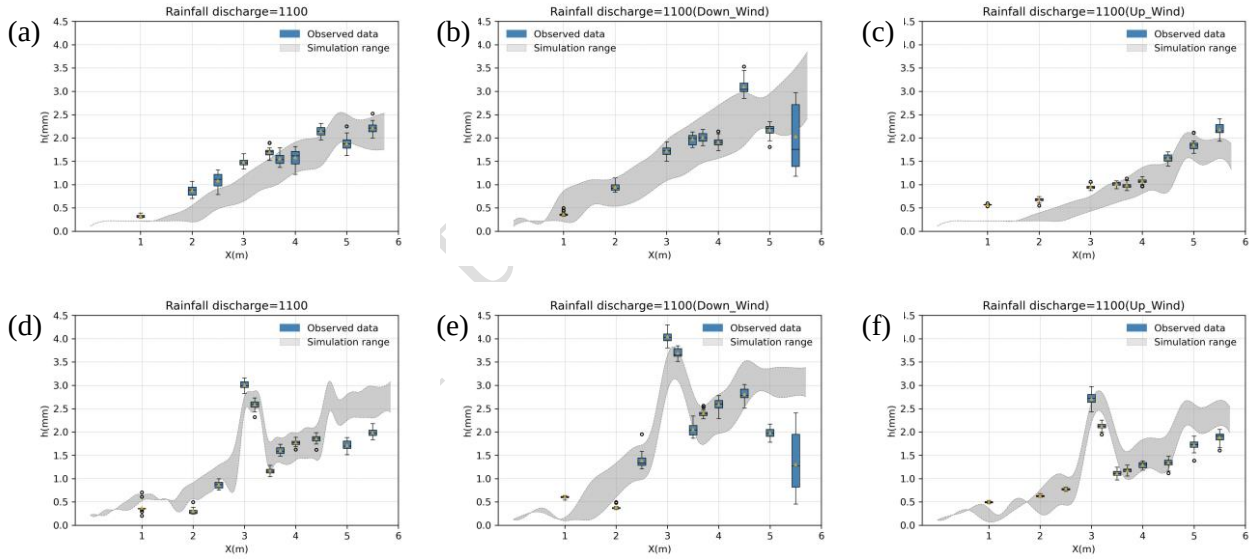

Figure A2. Simulated and measured WFD under the rainfall event with flow of 1100L/h: (a) ND surface without wind, (b) ND surface with downwind, (c) ND surface with upwind, (d) DE surface without wind, (e) DE surface with downwind, (f) DE surface with upwind. Noted: the grey band denotes ensemble simulated results with a range of varying manning's roughness.